Multiscale Membrane Models

Liu, Yang

DOI:
10.33612/diss.136221782

Chapter 1

Introduction

Cell membrane

The biological membrane

Biological membranes are basic structural elements of living cells. They act as selectively permeable barriers distinguishing the inter and intracellular space and forming the limiting boundary of the cell. In eukaryotic cells, the intracellular membranes also compartmentalize cells into organelles, so that these specialized subunits within cells can carry out their specific functions. Biological membranes usually consist of a lipid bilayer in combination with peripheral and integral proteins. The lipids act as a fluid matrix for proteins to laterally diffuse and rotate, and interact with the proteins for different physiological functions. In this way, the bilayer membrane is able to control a variety of cellular processes, such as cell adhesion, ion conductivity and cell signaling.

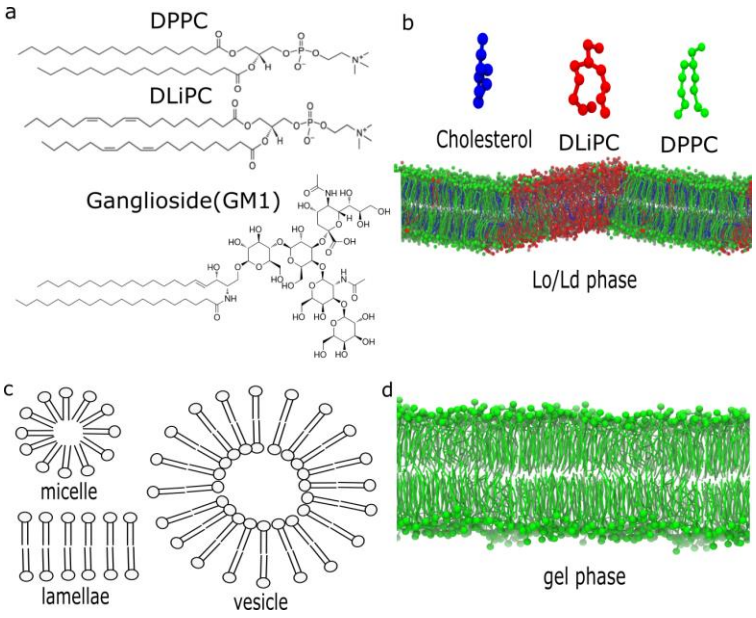

Figure 1. Illustrations of lipids and membranes. a) Chemical structures for Dipalmitoylphosphatidylcholine (DPPC), Dilinoleoylphosphatidylcholine (DLiPC) lipids and GM1 (monosialotetrahexosylganglioside). The chemical structure of lipids are download from https://en.wikipedia.org/wiki. b) Snapshot from simulations showing liquid-ordered (Lo, mostly DPPC and cholesterol) versus liquid-disordered (Ld, mostly DLiPC) packing of lipids. c) Examples of different lipid aggregation states. d) Snapshot from simulation of DPPC gel phase.

The lipids that constitute the cell membranes are small amphipathic molecules, usually consisting of two hydrocarbon tails and one polar head. The head structure typically possesses a

negatively charged phosphate group and is connected to another polar group, such as the positively charged choline in the case of zwitterionic phosphatidylcholines (e.g. Dipalmitoylphosphatidylcholine, DPPC) (Figure 1a). The lipid acyl tail structures vary in both chain length (the number of carbons in the fatty acid tail) and degree of saturation. A lipid can be entirely saturated (e.g. DPPC), implying that all of the carbons in the tail are connected by single bonds, or unsaturated (e.g. Dilinoleoylphosphatidylcholine, DLiPC), implying that there are one or more double bonds connecting the tail carbons (Figure 1a). In an aqueous environment, lipids can self-assemble into monolayer or bilayer structures such that the polar heads are exposed to the aqueous surrounding while shielding their apolar tails. Depending on the relative size of the lipid head groups versus the tail volume, they adopt a wide variety of aggregation states including micelles, lamellae and vesicles (Figure 1c).

Remarkably, most cellular membranes contain many different lipid types, with more than 1000 reported for the plasma membrane[1]. It is rather plausible that such a rich variety in lipid types gives rise to a heterogeneous distribution in the plane of the membrane. Indeed, already in the 1970s, Stier et al.[2] demonstrated the idea of membrane micro-domains or non-homogeneous cell membranes. Nowadays, it is commonly believed that the phase separation and phase behavior of lipids play an important role in membrane function. The liquid crystalline phase is the most common phase in most of the eukaryotic membranes, resembling a 2-dimensional fluid with the lipids freely diffusing in the plane of the membrane. Among the liquid crystalline phase, the liquid disordered (Ld) phase exhibits disordered packing in the lipid tails and the liquid-ordered (Lo) phase shows more ordered packing (Figure 1b). This is because of the presence of cholesterol in the Lo phase; cholesterol straightens out the saturated lipid tails as much as possible and keeps the carbon-carbon bonds in the trans-state. The inflexibility of the sterol ring thus rigidifies the overall membrane, increasing the order and bilayer thickness. The distinction in packing between the ordered phase and disordered phase may cause their phase separation. Whether Lo/Ld phase coexistence is observed depends on the temperature and lipid composition. In the ordered regions, both proteins and lipids diffusion is largely limited. Another ordered lipid phase is the gel phase. The gel phase is formed in the absence of cholesterol when the temperature is low enough to make it favorable for the lipid tails to remain all-trans (Figure 1d). In the gel phase, lipids are no longer fluid, consequently lateral diffusion in the gel phase is about 100 times slower than in the fluid phases.

In accordance with the idea of coexisting lipid phases, Estep et al. proposed the concept of lipid rafts in model cell membranes, composed of sphingolipids and cholesterol[3]. These ordered nanodomains are presumably small and highly dynamic (sizes in the range from 10 to 200 nm and lifetimes of the order of $\sim 10^{-3}$ s), and have been implicated to be important for many cellular processes, such as trafficking, signal transduction, and entry of pathogens[4-7]. The phase separation between liquid-ordered and disordered regions in model membranes are regarded as a simplified process of raft formation in the living cell membrane, with the Lo domains in model membranes corresponding to the rafts in the cell membrane. However, compared to the phase separation in the model membrane, the raft formation in the cell is less stable and short-lived. Many experimental evidences were found to support the existence of rafts in model membranes. Using fluorescence microscopy, Veatch and Keller observed spontaneous lateral domain separation in unilamellar vesicles composed of a ternary mixture of DOPC (dioleoyl-phosphatidylcholine)/DPPC and cholesterol[8]. In ternary mixtures of DOPC/sphingomyelin/cholesterol, raft-like domain dynamic properties were observed in a certain range of cholesterol concentration through confocal fluorescence microscopy and fluorescence correlation spectroscopy[9]. Baumgart el al. observed long-range domain ordering in the form of locally parallel stripes in giant unilamellar vesicles through high-resolution fluorescence imaging[10]. Structures similar to Lo and Ld domains found in model membrane systems are also observed in giant plasma membrane vesicles[11-12]. Apart from those, some important raft-like properties are found in native erythrocyte membranes by in situ atomic force microscopy experiment[13].

One of the classes of lipids that is believed to be enriched in lipid rafts are gangliosides (GMs). GMs are anionic glycosphingolipids, commonly found in body fluids, tissues and particularly abundant in the nervous system. They are primarily observed in the extracellular surface of the plasma membrane[14], and have been of special interest ranging from fundamental science to clinical study, serving as specific determinants in cellular recognition, receptors for certain hormones and bacterial and cell-to-cell communication. GMs manifest both pronounced hydrophobicity and hydrophilicity, with two ceramide tails and a charged saccharide head. GMs differ from each other by the sugar head structure. For example, GM1 (monosialotetrahexosylganglioside) has a head composed of 5 sugar monomers (Glucose, N-acetylgalactosamine, N-acetylneuraminic acid and two Galactose sugars) and two ceramide tails (Figure 1a). The hydrophobic moiety includes a sphingosine, composed of a long amino alcohol,

2-amino-1, 3-dihydroxy-octadec-4-ene, and connected to a fatty acid through an amide linkage. Because of their big saccharide head and saturated tail structure, GM1s partition into the ordered nanodomains, and may form nanoclusters with reduced lipid mobility in the plasma membrane[15].

Computational microscopy

Molecular dynamics (MD) has emerged as a unique and indispensable tool to complement conventional experimental approaches. It is able to describe the target system at atomic resolution and act like a "computational microscope"[16]. MD has been proven to be a powerful method for investigating a variety of biological systems. Besides, MD is not merely an in silico 'imaging' technique and can also be used to investigate dynamics, interactions, conformational changes, etc. Compared with the experimental approach, there are multiple advantages in computational models. MD enables precise control of the laboratory (or simulation) environment and allows the target resolution to go down to the motion of individual atoms. Besides, various alchemical tricks can be realized to calculate the thermodynamic driving forces. However, MD also has its limitations. One of the important drawbacks is the limited time and spatial scale of the simulated systems. Given the tremendous developments in both the software and hardware industry over the previous decades, the accessible spatio-temporal scales are largely enhanced. Nowadays, a model as large as HIV-1 capsid[17] and time scales on the order of microseconds (BPTI and gpW protein[18]) can be realized in all-atom simulations.

The essence of the success in MD lies in the high quality of the underlying force fields. In lipid membrane simulation, there are a variety of all-atom (AA) force fields, although the most famous of them fall into four families: CHARMM[19], AMBER[20], Slipids[21], and GROMOS[22]. They are broadly similar with respect to the potential functions (see section 1.3). The parameters of these potential functions, which define the force field, are mainly based on quantum mechanics (QM), NMR and X-ray diffraction data, In addition, thermodynamic properties of model compounds are used to calibrate the interactions, e.g. enthalpies and free energies of solvation.

After decades of development, simulations of the lipid membrane are able to provide a decent agreement with available experimental data (within the experimental uncertainty) for many membrane properties, e.g. area per lipid, deuterium order parameter, lipid diffusion rates, membrane bending constant to name but a few. This accomplishment was not achieved overnight. The initial configurations of lipids are primarily obtained from neutron and X-ray scattering and from NMR microscopy[23] and the partial charge is commonly acquired from ab initio calculation[24]. After decades of development and improvement, all of the force fields listed above successfully capture the balance of chemical-specific interactions of lipids to reproduce experimental

observables and can be used to investigate a variety of biomolecular processes. As an example relevant to this thesis, the phase separation or raft formation can be nowadays realized in AA simulations of membranes composed of DOPC, DPPC, and cholesterol[25].

Even though the AA simulations have successfully reproduced these biophysical properties of membranes, the accessible time and system size are still limited. Instead of computing interactions between AA pairs, combining atoms into single effective interaction sites in a so-called coarse-grain (CG) simulation can dramatically reduce the number of particles in the system. Besides, the high-frequency motions present in AA simulations (e.g. vibration of hydrogen bonds) are absent in the CG systems, allowing the use of larger integration time steps. In addition, the coarser representation of the interaction sites also produces a smoother potential energy surface and makes it easier to reach the global minimum of the system. Therefore, compared with AA simulations, computational efficiency has increased by orders of magnitude in CG simulations. Depending on the level of coarse grain in the system, simulations can easily reach effective real times of microseconds to milliseconds.

In the field of lipid membrane simulation, there are a number of available CG force fields. The most widely used are the Martini force field[26], the Shinoda/Devane/Klein (SDK) force field[27], and the Electrostatics-Based (ELBA) force field[28]. The Martini force field is the most famous CG force field, and a more detailed description will be given later. The Martini force field has already been used to simulate raft formation in a membrane composed of DPPC and DLiPC and cholesterol more than a decade ago, showing good agreement with experimental data[29-30]. The SDK force field uses softer interaction potentials, allowing for a good reproduction of heats of vaporization and surface tensions. This force field has mainly been used to investigate the phase behavior of lipid monolayers, vesicle fusion, and membrane partitioning of fullerenes. The ELBA force field focuses on capturing important electrostatic interactions (lipid−water interactions), where the water is modeled with soft sticky dipole potentials and incorporating point charges or point dipoles in lipid beads. Therefore, this force field enables a more accurate description of the electrostatic interactions compared with other CG models, at the cost of a reduced efficiency.

Molecular dynamics

Equations of motion

The idea of molecular dynamics was first proposed by Alder & Wainwright in the early 1950s as a technique to simulate a system with a number of colliding hard core particles[31]. The definition of the particles was further extended to be defined with continuous potentials in uniform time steps by Rahman[32]. Then time development of a system of particles is reproduced by simply solving Newton's laws of motion:

$$m_i \frac{d^2 r_i(t)}{dt^2} = F_i \quad (1)$$

$r_i(t), m_i$ and F_i represent the position, mass and the momentary force of particle i. The force is obtained from the derivative of potential V_i felt by the particle i:

$$F_i = -\frac{\delta V_i(t)}{\delta r_i(t)} \quad (2)$$

The calculation of the potential is a central part of the molecular dynamics algorithm, the nature of which is quantum mechanics. However, due to the big size of the most biomolecular systems, it is extremely expensive to directly derive the potential from the first principles and hence the potential is commonly represented by some semi-empirical classical force fields. These force fields can be parameterized either from quantum mechanical calculations or through fitting to well known experimental observables. The calculation of the potential between every pair of interaction sites in the system is still very time-consuming, so the interactions beyond a cutoff distance are neglected. Besides, since the attractions of the Lennard–Jones (LJ) potential decrease with $(1/r)^6$ and Coulombic potential decrease with $1/r$, only a small portion of the potential beyond the cutoff is ignored. Details of the force field used in this thesis will be discussed in the next section.

Equation 1 is solved numerically to predict the positions of all the particles in the system in every step of the simulation period. Therefore, a trajectory of the system is produced and we can apply statistical mechanics to compute the macroscopic properties. To integrate the equation of motion, different strategies can be applied and we will focus on two of them implemented in the GROMACS package[33] (the MD software used in this thesis): md and sd integrators.

The md integrator in GROMACS is using the leapfrog algorithm to solve the differential equation 1. This algorithm updates positions and velocities of molecules at equidistant time points Δt:

$$r_i'(t+\frac{1}{2}\Delta t) = r_i'(t-\frac{1}{2}\Delta t) + r_i''(t)\Delta t \quad (3)$$

$$r_i(t+\Delta t) = r_i(t) + r_i'(t+\frac{1}{2}\Delta t)\Delta t \quad (4)$$

r_i' and r_i'' are the first and second derivative of the coordinates with respect to time. Velocity-Verlet algorithm, closely related to leapfrog, is also implemented in GROMACS. The main difference between the two algorithms is that Vertlet calculates both the positions and velocities at the same frame. These integrators are deterministic, suggesting that two simulations possessing the same starting states can reproduce the same trajectories.

Another integrator implemented in GROMACS software is the leapfrog based stochastic dynamics (sd). The noise and friction terms are added into Newton's laws of motion:

$$r_i'(t+\frac{1}{2}\Delta t) = r_i'(t-\frac{1}{2}\Delta t)\alpha_i + r_i''(t)\Delta t + \sqrt{\frac{k_B T}{m_i}(1-\alpha_i^2)n_i^G} \quad (5)$$

$$\alpha_i = (1-\frac{\gamma_i}{m_i}\Delta t) \quad (6)$$

$$r_i(t+\Delta t) = r_i(t) + r_i'(t+\frac{1}{2}\Delta t)\Delta t \quad (7)$$

m_i, γ_i, and n_i^G are mass, friction constant and added noise of particle i extracted from the standard normal distribution. k_B and T are the Boltzmann constant and the temperature of the system.

Simulation settings

Ensemble properties, like temperature and pressure, cannot be attributed to individual atoms, and are determined by a huge amount of molecules. A momentary microscopic temperature of the system is defined as:

$$T(t) = \sum_{i=1}^{N} m_i v_i(t)^2/(N_f k_B) \quad (8)$$

where temperature is closely related to the kinetic energy of the atoms. N_f, k_B, v_i and m_i are the number of degrees of freedom, Boltzmann's constant, atom velocity and mass, respectively. The effective temperature is an ensemble average of the temperature throughout the simulation:

$$T = < T(t) > \quad (9)$$

Typically, the initial temperature is set by assigning random velocities with a gaussian distribution. Ideally the temperature of the system is maintained throughout the simulation.

However, because of the force truncation errors in the integration algorithm and other artificial factors, a thermostat is needed to keep the constant temperature. For example, a weak coupling scheme (also denoted Berendsen thermostat[34]) is applied through scaling the atom velocity with:

$$\lambda = \sqrt{1 + \Delta t/\tau_T(T_0/T(t) - 1)} \quad (10)$$

Δt, τ_T and T_0 are time step, temperature coupling time constant and targeted temperature. This scheme is able to generate an exponential relaxation to the reference temperature. Other extended temperature thermostats, like the Nose-Hoover algorithm[35], were proposed that can produce a proper canonical ensemble.

In addition, the pressure in the system can be derived through the virial theorem:

$$p = 2(\sum_{i=1}^{N} r_i \otimes F_i - \sum_{i=1}^{N} m_i v_i \otimes v_i)/V \quad (11)$$

where m_i, v_i F_i and $r_i$are the mass and velocity, force and coordinate of the atom i. N and V are the number of particles and volume of the simulation cell.

Similar to temperature thermostat, a weak pressure coupling scheme[34] is applied through scaling the coordinate and box size by:

$$\mu = \sqrt[3]{1 + \Gamma(p - p_0)\Delta t/\tau_p} \quad (12)$$

where Δt, Γ, τ_p and p_0 are time step, compressibility, pressure coupling time constant and targeted pressure. Alternative barostats (e.g. Parinello-Rahman scheme[36]) are also available.

Apart from a thermostat and barostat, periodic boundary conditions are also commonly applied to MD simulations. Compared to the real macroscopic structures, the simulated systems are considerably small. If one would simulate an isolated system, many of the molecules are exposed to the vacuum environment - an unnatural boundary surface. To solve this problem, periodic boundary conditions are introduced to approximate the infinite box. The molecules are placed in a simulation box, and when they cross the boundary, they reappear on the opposite side with the same velocity. During the simulation, only the properties of the center box need to be recorded and propagated and the surrounding boxes are just image copies.

The Martini force field

The Martini force field is one of the most famous CG force fields, developed by Marrink and co-workers[37]. It is computationally fast, easy to apply and flexible enough to cover a broader range of applications without reparametrizing the model each time[38]. This force field was initially developed to simulate membrane lipids, and gradually extended to proteins[39], carbohydrates[40], DNA[41] and various polymers. The hallmark of the Martini force field is that the beads are parameterized to reproduce experimental thermodynamic quantities, e.g. oil/water partitioning coefficients, the degree to which crucially contributes to biomolecular processes such as lipid self-assembly, peptide–membrane binding, and protein-protein recognition[38]. Therefore, the experimental based parameterization makes the model perform closer to realistic behavior.

The Martini force field uses the Lennard–Jones (LJ) 12/6 interaction function and the normal electrostatic Coulombic potential to calculate the short-range nonbonded interactions. The interactions between interaction sites i and j are described by:

$$U_{LJ}(r) = 4\,\epsilon_{ij}[(\sigma_{ij}/r)^{12} - (\sigma_{ij}/r)^{6}] \quad (13)$$

$$U_{electrostatic}(r;q) = q_i q_j/(4\pi\varepsilon_0\epsilon_r r) \quad (14)$$

With parameters, q and r describe particle charge and distance between interaction sites i and j. σ_{ij} represents the effective minimum distance of approach between two particles, ϵ_{ij} the strength of their interaction, $\epsilon_0$the dielectric permittivity of vacuum and ϵ_r relative permittivity. The original Martini force field[37] uses a cutoff of 1.2 nm. The LJ potential is smoothly shifted to zero between 0.9 nm and 1.2 nm and the Coulomb potential is shifted from 0 nm to 1.2 nm. The Martini force field in modern setting[42] uses a cutoff of 1.1 nm and both LJ and Coulomb potentials are shifted to zero at the cut off using potential modifiers.

The bonded interactions are described by a weak harmonic potential:

$$V_{bond}(r) = 1/2k_{bond}(r - r_{bond})^2 \quad (15)$$

k_{bond} and r_{bond} are bond force constant and equilibrium bond distance respectively. LJ interactions are excluded between bonded beads. To reproduce chain stiffness, a weak harmonic potential of the cosine type is introduced for the angles

$$V_{angle}(\theta) = 1/2k_{angle}[\cos(\theta) - \cos(\theta_0)]^2 \quad (16)$$

k_{angle} and θ_0 are the angle force constant and equilibrium angle between consecutive bonds, respectively. The improper dihedral angle potential is applied for more complicated geometries to prevent out of plane distortions

$$V_{di}(\theta) = 1/2k_{di}(\theta - \theta_{di})^2 \quad (17)$$

where k_{di} and θ_{di} are angle force constant and equilibrium dihedral angle, respectively. A proper torsional dihedral angle is applied:

$$V_d(r) = k_{tor}[1 + \cos(m\varphi - \varphi_0)] \quad (18)$$

where k_{tor}, m, φ_0 and φ are the torsion force constant, the multiplicity of the torsional dihedral angle, the equilibrium dihedral angle and the actual value of the dihedral angle, respectively.

GROMOS force field

CG simulation is fast and efficient, however, atomistic details and a certain level of accuracy are sacrificed. Thus, the AA model simulated with the GROMOS force field is also included in this thesis. The GROMOS force field is a united force field, in which aliphatic hydrogens are not taken into account explicitly. For example, in lipids, the methyl (CH3) and methylene (CH2) atoms are represented by a single site, hence reducing the interaction sites from 4 to 1 and 3 to 1, respectively. Therefore, compared with all-atom membrane simulation, computational efficiency is higher. The GROMOS force field is primarily parameterized with respect to experimental data on small molecules, reproducing the free enthalpies of hydration and apolar solvation for a range of compounds[43]. It has been successfully applied in a large scale of applications, such as protein folding, biomolecular association, membrane formation, and transport over membranes[44].

The GROMOS force field also uses the LJ 12/6 interaction function as described in Equation 13 and a plain cutoff scheme is used to reduce the computational cost. A reaction field is used to represent the long-range contribution of the Coulomb interaction:

$$U_{RF}(r; q) = q_i q_j/(4\pi\varepsilon_0\epsilon_1)[-0.5 * \frac{C_{rf} r^2}{R_{rf}^3}] \quad (19)$$

where

$$C_{rf} = (2\epsilon_1 - 2\epsilon_2)(1 + \kappa R_{rf}) - \epsilon_2(\kappa R_{rf})^2 /[(\epsilon_1 + 2\epsilon_2)(1 + \kappa R_{rf}) + \epsilon_2(\kappa R_{rf})^2] \quad (20)$$

With ϵ_0 and ϵ_1 represent the dielectric permittivity of vacuum and the relative permittivity of the medium, in which the atoms are embedded in. ϵ_2 and κ are the relative permittivity and inverse Debye screening length of the medium outside the cutoff sphere defined by R_{rf}, respectively. The nonbonded interactions are cut off at a distance of 1.4 nm.

The bonded interactions are described by a weak harmonic potential:

$$V_{bond}(r) = 1/4k_{bond}(r^2 - r_{bond}^2)^2 \quad (21)$$

where k_{bond} and r_{bond} are bond force constant and equilibrium bond distance respectively.

The GROMOS force field uses the same angle and improper dihedral potential functions as described in Equations 17 and 18. In addition, a proper torsional dihedral angle is applied using the trigonometric function:

$$V_{tor}(r) = k_{tor}[1 + \cos(\delta)\cos(\varphi m)] \quad (22)$$

where k_{tor}, δ, m and φ are the torsion force constant, phase shift (either 0 or π), the multiplicity of the torsional dihedral angle and the actual value of the dihedral angle, respectively.

Hybrid force field

Many biomolecular systems are computationally challenging to simulate with the molecular dynamics technique due to their large size and need for long time scales. Despite the increasing computer power, the current and near-future computational capability is still falling short. Even though the computational efficiency is largely increased in CG simulation, the molecular details are, however, sacrificed during the process. With the idea of keeping the best of both worlds (AA and CG), researchers start to consider combining AA and CG resolutions in one system, describing different parts of the system with different resolution scales. For example, a straightforward way to design a multiscale simulation is representing the solutes (proteins, membranes, etc.) in AA resolution, while the solvents are in CG resolution (e.g. PACE[45]). One of the major limitations of such multiscale approaches is the need for deriving accurate cross interactions between the two levels of resolution.

To alleviate such problems, efforts have been made to combine the Martini and GROMOS force field through a virtual site scheme proposed by Rzepiela et al.[46]. The main idea of this hybrid scheme is that the virtual sites are built on the center of mass of the corresponding atoms and these virtual sites can interact directly with other coarse grain beads through the Martini interaction scheme. CG and AA molecules interact with themselves using their own interaction schemes and no cross interaction between the two resolutions is involved. The electrostatic coupling in the hybrid scheme was further tested and updated by Wassenaar et al.[47]. This hybrid scheme is also applied using adaptive resolution simulation to simulate atomistic DNA[48] and protein[49] molecules

in a Martini solvent environment.

Replica and Hamiltonian exchange

To increase the sampling speed in simulations, a large number of enhanced sampling techniques exist. One of those that is relevant for this thesis is the replica exchange method (REM). REM, also called parallel tempering, was originally introduced by Sugita Y. et al.[50] in 1999 and has been extended to different forms for enhanced molecular sampling[51-53]. The basic idea is to run a number of independent simulations (replicas) at different temperatures, and exchange configurations between the replicas. Typically, the energy landscape of biomolecular systems contains many local minima that are separated by high energy barriers. These free energy barriers, that are hardly crossed in traditional MD simulation, are overcome in the REM replicas running at high temperatures, the conformations of which are exchanged to the rest of replicas. Hence, the sampling efficiency is enhanced. Since the conformation exchange satisfies the detailed balance condition, the correct thermodynamic ensemble is maintained within each individual replica. Based on the same idea, the Hamiltonian replica exchange method (HREM) was developed as an extension of the temperature REM, in which each replica uses different interaction potentials (or different resolutions between AA and CG) instead of the different temperatures. The faster sampling at CG replicas can accelerate the sampling efficiency of replicas at AA resolution, as has been demonstrated in a proof of principle paper based on the GROMOS/Martini hybrid scheme[54].

Aim and outline of this thesis

The aim of this thesis is divided into two parts. The first one is to investigate the distribution of GMs in ternary model membranes and its effects on membrane phase separation. The second one focuses on developing new multiscale methods, which can be used to enhance the sampling efficiency through Hamiltonian replica exchange or to increase computational efficiency by replacing part of the system by CG resolution.

In Chapter 2, we have studied the effect of GM on phase separation. As we know, GMs are believed to be imperative for many cellular processes, such as trafficking, signal transduction, and entry of pathogens. Despite the important role of GM in the biomembrane system, a detailed understanding of the organization of GM-rich membranes is still lacking. Here, we use CG molecular dynamics simulations to investigate the effect of GMs on phase coexistence in a model

membrane composed of DPPC, DLiPC and cholesterol. We found that a certain amount of GMs is able to destabilize the phase separation. Through investigating the influence of GMs on the conformational and structural properties of the ternary membrane, a reasonable mechanism of the destabilizing effect is proposed.

In Chapter 3, efforts have been made to develop a multiscale enhanced sampling scheme via the Hamiltonian replica exchange method. The multiscale configuration concurrently couple all-atomistic (GROMOS force field) and coarse grain (Martini force field) resolutions in one system and we expect that the fast sampling speed of the coarse grain replicas can guide and accelerate the all-atomistic replicas. We tested the efficiency of this procedure using a lutein/octane system and found that we can sample more trans/cis transitions than traditional simulations. Our new multiscale method can also be useful in the ongoing development of related multiscale and enhanced sampling simulations.

In Chapter 4, we propose another virtual site based multiscale scheme that can concurrently couple AA and CG resolutions in a membrane simulation. We combined modified GROMOS and CHARMM force field with the Martini force field to simulate multiscaled bilayer membranes. The input parameters were carefully tuned to represent the correct conformational and dynamical characteristics of the membrane and the computational efficiency is greatly increased, especially in the case of a vesicle.

In Chapter 5 and 6, the virtual site hybrid scheme introduced in chapter 4 was applied to study the phase separation process and vesicle dynamics, respectively. The Martini force field has successfully captured spontaneous separation of ternary membranes into a liquid-disordered and a liquid-ordered phase that can hardly be reached by simulation with atomistic details. Therefore we applied the VS hybrid method on such a ternary membrane (composed of DPPC, DLiPC and cholesterol) and expected the phase separation of the CG leaflets to accelerate and guide this process in the AA leaflets. Simulating a vesicle in AA resolution and studying its dynamic properties is very expensive for current computational power. Therefore, we applied the VS hybrid method to vesicles in which the inner leaflet was at the AA resolution and the outer leaflet at CG resolution. We considered vesicles with sizes ranging from 15 nm to 25 nm and computed the dynamic relaxation properties of the AA lipid tails in the hybrid conformations.

The thesis is concluded with a summary/outlook section, recapitulating the main results obtained and sketching the possible future developments in this field.